Improved Broadband Emissivity Parameterization for Water Vapor Cooling Rate Calculations

WENYI ZHONG AND J. D. HAIGH

Space and Atmospheric Physics Group, Blackett Laboratory, Imperial College, London, United Kingdom

(Manuscript received 31 January 1994, in final form 1 June 1994)

ABSTRACT

Reference transmissivities based on line-by-line calculations have been computed for a wide range of homogeneous paths of water vapor. A new approach is employed in which wideband emissivities are directly fitted to the line-by-line reference calculations without using the intermediate step of narrowband models. A significant improvement in accuracy is obtained over previous schemes. Compared with line-by-line computed fluxes and cooling rates (without continuum absorption) for the standard middle-latitude summer (MLS) profile, the maximum error in fluxes is 1.5 W m^{-2}; agreement is within 1% in fluxes and within 0.11 K/day, or 5%, in cooling rate. Unlike most published water vapor continuum schemes, which use the Roberts et al. model, the authors have reformulated the treatment of the water vapor continuum by producing a new parameterization based on the semiempirical model of Clough et al. This results in ~7.5 W m^{-2} difference in calculated radiative fluxes at the tropopause, and maximum difference in fluxes can approach 15 W m^{-2} in the troposphere for the MLS atmosphere.

1. Introduction

The emissivity approach is well established as an efficient and accurate method by which to approximate water vapor longwave radiative fluxes and cooling rates in atmospheric modeling. Its implementation has two requirements: first, good reference transmissivities must exist, and, second, they must be put into an appropriate form for the calculation of fluxes. Rodgers (1967) investigated the use of emissivity in atmospheric radiation calculations and found it possible to represent it as an analytical function of absorber amount. Ramanathan and Downey (1986, hereafter RD) indicated that the fundamental limitation of an isothermal emissivity was one of the main sources of error in atmospheric radiation calculations and introduced nonisothermal water vapor emissivity and absorptivity formulations. They derived emissivity and absorptivity expressions from reference calculations using a narrowband model (NBM), which satisfied the asymptotic conditions of absorber amount. Morcrette et al. (1986, hereafter MSF) concluded that the Rodgers (1967) emissivity approach could give accurate results provided that both the temperature and pressure dependencies were incorporated in the narrowband calculations; they used the method of least squares to fit the reference transmissivities calculated by the Malkmus narrowband model to the strong line approximation (SLA) for each 5 cm^{-1} spectral interval, forcing the SLA to have correct pressure and temperature dependencies. A Padé approximant was used as the functional form for the transmissivity. While the RD and MSF methods are accurate, they are based on reference calculations made using the Malkmus narrowband model (1967), and the procedure whereby the pressure and temperature dependencies are incorporated is either very complex or must rely on empirical adjustments. It would be more straightforward and more accurate to adopt line-by-line calculations for the reference emissivities. Since a line-by-line model includes all the necessary information on the absorption line parameters and line shapes, and the angular integration can also be included accurately, its limitation derives solely from uncertainties in the laboratory measurements. In this paper, we use a line-by-line model to calculate all the required reference transmissivities for water vapor, and a simple expression is fitted directly to the line-by-line calculated reference emissivities over wide spectral intervals so that the correct pressure and temperature dependencies of the transmissivities are incorporated. For the water vapor continuum a new parameterization based on the work of Clough et al. (1989) (the CKD model hereafter) is developed for all the spectral intervals. Finally some comparisons between the results of the emissivity model and line-by-line computed fluxes and cooling rates are presented.

2. The infrared radiation scheme

The framework of the longwave radiation scheme used in the European Centre for Medium-Range Weather Forecasts (ECMWF) forecasting model (Morcrette 1989) has been adapted for our emissivity

Corresponding author address: Dr. Wenyi Zhong, Imperial College of Science, Technology and Medicine, Space and Atmospheric Physics Group, Blackett Laboratory, London SW7 2BZ, United Kingdom.

calculations. The present ECMWF radiation scheme was developed from the application of a narrowband model of as high as possible resolution (5 cm^{-1}) and compared with line-by-line calculations and in situ measurements (Morcrette 1991). The scheme is of high accuracy and efficiency and incorporates effectively a representation of cloud radiative properties. It has successfully corrected most deficiencies of previous ECMWF schemes. A brief review of its longwave method follows.

As in most longwave radiative transfer calculations for weather forecasting and climate modeling, the ECMWF longwave radiation scheme includes all the vibration–rotation bands for H_2O (0–2820 cm^{-1}) and water vapor continuum absorption (350–1250 cm^{-1}), the 15-μm band of CO_2, and the 9.6-μm band of O_3. It also calculates the minor bands of CO_2 in the 800–1200 cm^{-1} region but ignores the minor trace gases and other bands of O_3. A band emissivity method, developed from the Malkmus narrowband model (MSF), is used to evaluate the longwave fluxes. The LW cooling rate in the atmosphere is given by

$$\frac{dT}{dt} = \frac{g}{c_p}\frac{d\sum_{i=1}^{N} F_i}{dp}, \tag{1}$$

where T is the atmospheric temperature, F_i is the net upward longwave radiation flux in the ith spectral interval, N is the total number of spectral intervals, c_p is the specific heat of dry air at constant pressure, and g the acceleration due to gravity. Ignoring scattering and assuming local thermodynamical equilibrium, upward and downward fluxes can be expressed by integrating the radiative transfer equation (e.g., see Goody and Young 1989) as

$$F_i^{\uparrow}(p) = [B_i(T_s) - B_i(T_{0+})]t_{B_i}^d[u(p_s, p), T_u(p_s, p)] + B_i(T_p) + \int_{B(T_{0+})}^{B(T_p)} t_{dB_i}^d[u(p, p'), T_u(p, p')]dB_i(T_{p'})$$

$$F_i^{\downarrow}(p) = [B_i(T_0) - B_i(T_\infty)]t_{B_i}^d[u(p, 0), T_u(p, 0)] - B_i(T_p) - \int_{B(T_p)}^{B(T_t)} t_{dB_i}^d[u(p', p), T_u(p', p)]dB_i(T_{p'}), \tag{2}$$

where B_i represents the Planck function (including the π factor) integrated over the ith spectral interval (in units of W m^{-2}), T_s is the surface temperature, T_{0+} that of the above-surface air, T_p the emitting temperature at the level of pressure p, T_t that at the top level, and T_∞ that of space above the top level. Here $T_u(p, p')$ is the mass-weighted mean temperature of the atmospheric path between pressures p and p' and affects the transmission through the temperature dependence of the absorption line parameters in the ith interval. Also, $u(p, p')$ is the absorber amount between p and p'; t_B^d and t_{dB}^d are two normalized wideband transmissivities weighted by the Planck function and the derivative of the Planck function. The superscript d represents the diffuse transmission. As below, t_B^d and t_{dB}^d can be expressed with a line-by-line model:

$$t_{B_i}^d(up, T_u, T_p) = \frac{2\int_{\Delta\nu_i} B_\nu(T_p)\int_0^1 \exp\{[-\sum_l S_l(T_u)f_l(\nu, p, T_u)u]/\mu\}\mu d\mu d\nu}{\int_{\Delta\nu_i} B_\nu(T_p)d\nu}$$

$$t_{dB_i}^d(up, T_u, T_p) = \frac{2\int_{\Delta\nu_i} \frac{dB_\nu(T_p)}{dT}\int_0^1 \exp\{[-\sum_l S_l(T_u)f_l(\nu, p, T_u)u]/\mu\}\mu d\mu d\nu}{\int_{\Delta\nu_i} \frac{dB_\nu(T_p)}{dT}d\nu} \tag{3}$$

where $S_l(T_u)$ is the strength of the lth absorption line at frequency ν in the ith interval, $f_l(\nu, p, T_u)$ is the normalized line shape function for the lth line of the absorber gas, and μ is the cosine of the zenith angle.

The two types of emissivity, or emissivity and absorptivity, are defined as

$$\epsilon_1^i(up, T_u, T_p) = 1 - t_{B_i}^d(up, T_u, T_p)$$

$$\epsilon_2^i(up, T_u, T_p) = 1 - t_{dB_i}^d(up, T_u, T_p). \tag{4}$$

The single-parameter scaling approximation is used to find the pressure-weighted absorber amount,

$$\overline{up} = \int_{\text{path}} p du. \tag{5}$$

In the ECMWF longwave radiation scheme the whole infrared spectrum is divided into six intervals, of which three represent two regions each. In order to design a more flexible longwave radiation scheme (i.e., one into which more gases may easily be incorporated subsequently), we use only one combined band and split the other two so that there are eight longwave intervals; see Table 1.

TABLE 1. Longwave spectral intervals.

Number	Interval
1	0–350 + 1450–1880 cm^{-1}
2	350–500 cm^{-1}
3	500–800 cm^{-1}
4	800–970 cm^{-1}
5	970–1110 cm^{-1}
6	1110–1250 cm^{-1}
7	1250–1450 cm^{-1}
8	1880–3000 cm^{-1}

In the following sections we describe how the reference transmissivities for water vapor are computed using a line-by-line model and how the wideband models are fitted by a least squares method. The fluxes and cooling rates of different atmospheric profiles calculated by the wideband models are then compared with those computed by a line-by-line model.

3. Line-by-line reference transmissivities

With the recent rapid increase in computer power, it is now feasible to perform line-by-line calculations of transmissivities, fluxes, and cooling rates for many different atmospheric conditions. Because line-by-line models represent high-resolution spectral structure and accurately include the appropriate physics, they can be used as standards for the development of fast approximate algorithms for climate and weather prediction models (e.g., Chou and Arking 1980) and also as benchmarks for the intercomparison of radiation codes (e.g., Ellingson et al. 1991).

In the present work the line-by-line reference transmissivities are computed for homogeneous paths over a wide range of pressures, water vapor concentrations, and temperatures over each of the eight spectral intervals. A complete description of the line-by-line model (GENLN2) is given by Edwards (1987, 1988); a brief review follows. The temperature dependence of line strength in the model is expressed as

$$S(T) = S(T_0)\left(\frac{T_0}{T}\right)^m \frac{Q_\nu(T_0)\exp(-E_l/k_BT)}{Q_\nu(T)\exp(-E_l/k_BT_0)} \times \frac{1-\exp(-hc\nu/k_BT)}{1-\exp(-hc\nu_0/k_BT_0)}, \quad (6)$$

where the first term represents the ratio of the rotational partition functions, the second term the ratio of the vibrational partition function, the third the ratio of Boltzmann functions, and the final term the effects of stimulated emission; E_l is the energy of the lower state. The Voigt profile is used for all calculations in which the temperature and pressure dependence of the Lorentz line width α_L due to self-broadening and air broadening is expressed by

$$\alpha_L(p,T) = \left(\frac{T_0}{T}\right)^m [\alpha_{L_a}(p_s,T_0)(p-e) + \alpha_{L_s}e], \quad (7)$$

where α_{L_s} and α_{L_a} are the self-broadening and air-broadening half-widths, respectively, and e and p are the path partial and total pressures, respectively.

All line parameters including the line wavenumbers, line strengths, lower-state energies, Lorentz half-widths, and the coefficients of their temperature dependence are

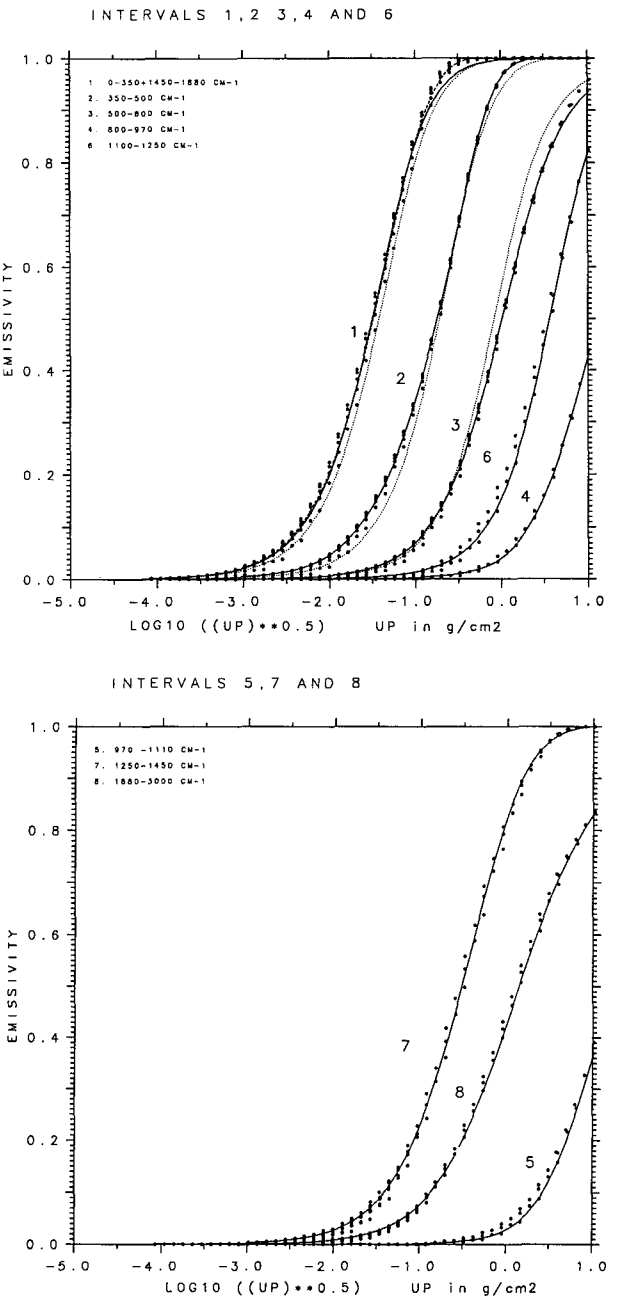

FIG. 1. Emissivity plotted against the logarithm of the square root of scaled absorber amount for (a) intervals 1, 2, 3, 4, and 6, and (b) intervals 5, 7, and 8. The dots represent the GENLN2 line-by-line calculations, the solid lines the least-squares fitting to the two-term Padé approximant, the dashed line the least squares fitting to the three-term Padé approximant for the strong band, 0–350 + 1450–1880 cm^{-1}, and the dotted lines the ECMWF results.

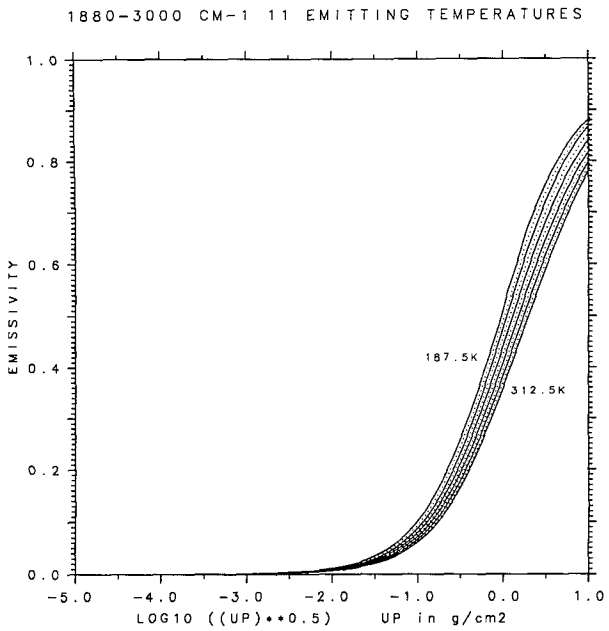

FIG. 2. Emissivity versus the logarithm of the square root of scaled absorber amount for interval 8 for the 11 emitting temperatures.

taken from the HITRAN database (Rothman et al. 1987). The spectral resolution is 0.01 cm^{-1}, and the wings of all lines within 25 cm^{-1} of the frequency under consideration are included. The integration over zenith angles is computed using a seven-point Gaussian quadrature. The reference transmissivities are computed according to Eq. (3) for homogeneous paths for 11 values of pressure between $\ln(p) = 7$ and $\ln(p) = 2$ (p in mb) with $\Delta \ln(p) = 0.5$; three values of T_u: 200 K, 250 K, and 300 K; 11 values of T_p from 187.5 to 312.5 K with step $\Delta T = 12.5$ K; and 20 values of absorber amounts from $\ln(u) = -8$ to $\ln(u) = 11$ (u in mol m^{-2}) with $\Delta \ln(u) = 1$. In the following section only those absorber amounts that are physically reasonable over the range of conditions in the troposphere and lower stratosphere are used for each pressure level (thus, for example, a pairing of high absorber amount with low pressure is not used).

4. Fitting wideband transmissivites to line-by-line calculations

Rodgers (1967) found that, over limited ranges of absorber amount, emissivity could be represented as a simple algebraic function of pressure-weighted absorber amount (u). For low absorber amount the formula was a four-term polynomial in $u^{1/2}$, and for high amounts a five-term polynomial in $\ln(u)$. The coefficients were found by a least squares procedure. However, a single formula could not be used to represent the whole range of possible absorber amounts. To represent the far-wing effects RD employed the SLA plus empirical terms. MSF developed the Rodgers technique by replacing polynomials with a single formula in terms of a Padé approximant; however, in order to obtain the correct pressure and temperature dependencies a correction had to be made to the SLA, using the method of Garand (1983), in each 5 cm^{-1} interval by an LSF to the optical depths calculated using a Malkmus NBM. The advantages of the Padé approximant are not only its speed, but also its accuracy and convergence properties (Fouquart and Bonnel 1980). In this work we find approximate expressions for wideband emissivity as a function of absorber amount by fitting not to NBM but directly to line-by-line calculations. We have compared the numerical behavior of the polynomial obtained by an LSF to some of the line-by-line calculated reference emissivities with the Padé approximant derived from the same polynomial and, as expected given the discussion above, found the latter to perform better.

Using a nonlinear least squares method, the following two-term Padé-like formula [Eq. (8)] is fitted to the line-by-line precomputed wideband reference emissivities for all the spectral intervals:

$$\epsilon(up, T_u) = [c_1(up)^{1/2} + up] \times [b_0 + b_1(up)^{1/2} + up]^{-1}; \quad (8)$$

and the transmissivity can be obtained from the following equation:

$$t(up, T_u) = [a_0 + a_1(up)^{1/2}] \times [b_0 + b_1(up)^{1/2} + up]^{-1}, \quad (9)$$

where coefficients c_i and b_i are determined by the LSF, and $a_0 = b_0$, $a_1 = b_1 - c_1$. The solid lines in Fig. 1a and 1b show the line-by-line calculations and the results of the LSF for the eight intervals, which are in general very good. For the strong absorption band 0–350 + 1450–1880 cm^{-1}, the three-term Padé approximation equation (10) gives a better fit for large optical depths than the lower-order equation (9);

$$t(up, T_u) = [a_0 + a_1(up)^{1/2} + a_2(up)] \times [b_0 + b_1(up)^{1/2} + b_2(up) + (up)^{3/2}]^{-1}, \quad (10)$$

see dashed line in Fig. 1a. Because the improvements are only at very large absorber amounts, they have

TABLE 2. Ratios $\frac{\bar{C}_s^i(260)}{\bar{C}_s^i(296)}$ for each spectral interval.

0–350 + 1450–1880	500–800	800–970	1110–1250	970–1110	350–500	1250–1450	1880–2820
1.5	1.9, 2.05	2.13	1.9	2.03	1.5	1.5, 1.35	2.35

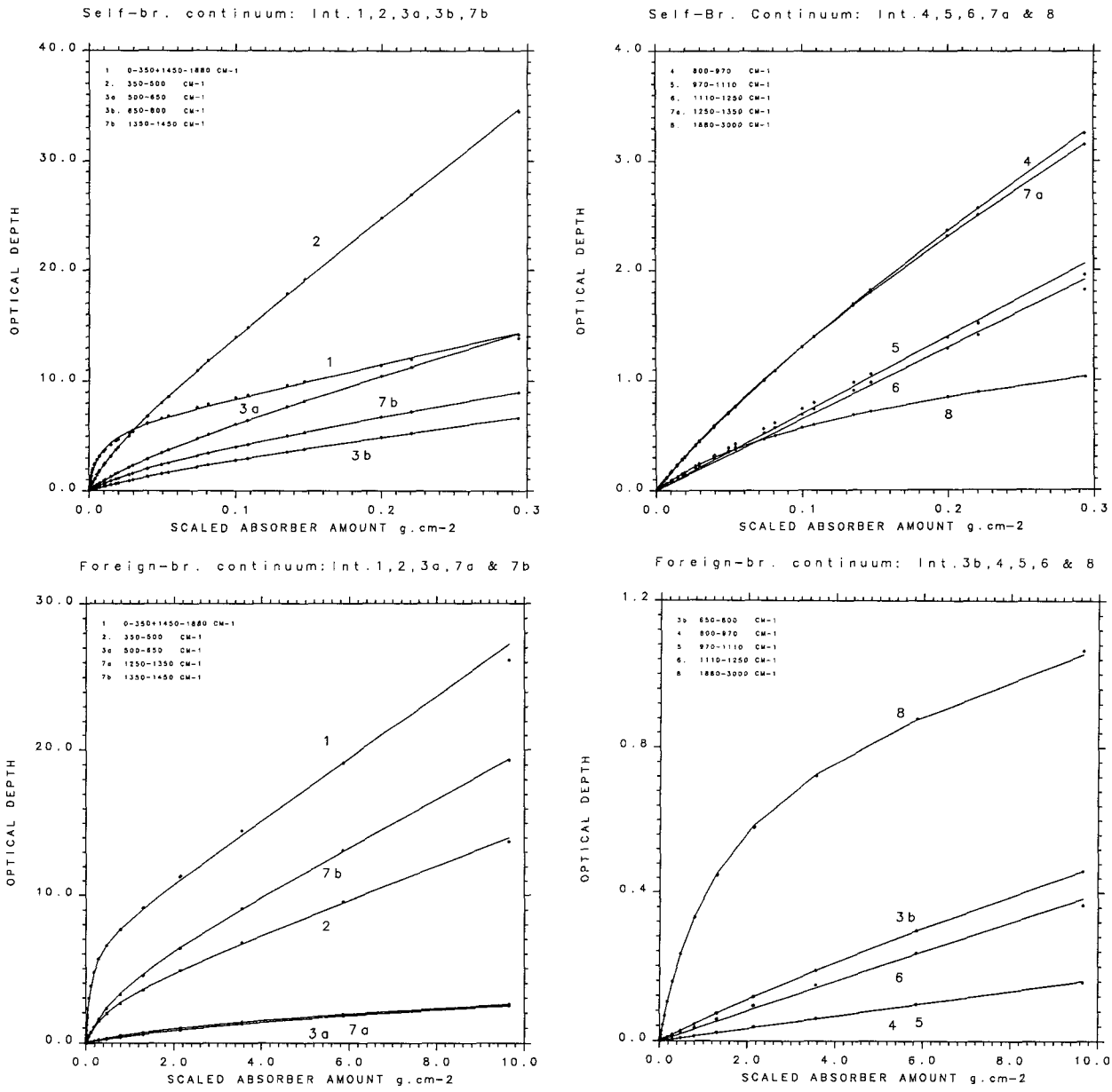

FIG. 3. Optical depth of water vapor continuum absorption versus scaled absorber amount. (a) Self-broadened continuum in the intervals 1, 2, and the two subintervals 3a and 3b of the interval 3 and one subinterval 7b of the interval 7; (b) self-broadened continuum in the intervals 4, 5, 6, 8, and the subinterval 7a; (c) foreign-broadened continuum in the intervals 1, 2, 3a, and 7b; (d) foreign-broadened continuum in the intervals 3b, 4, 5, 6, and 8. The dots are reference calculations obtained using the line-by-line method; the curves are least squares fitting.

very little effect on the flux and cooling rate calculations. So, in order to avoid an increase in computer time, the two-term Padé approximant, Eq. (9), is used for all spectral intervals:

We have compared our results with those of the ECMWF scheme (dotted lines in Fig. 1). It can be seen that their model slightly underestimates the water vapor absorption for the strong absorptive bands, for example, 0–350 + 1450–1880 and 350–500 cm^{-1} intervals, when compared with the GENLN2 calculations. This may be attributed to the deficiency of the 5 cm^{-1} narrowband model to account for the far-wing effect. For the weaker intervals of 500–800 and 970–1110 cm the ECMWF Padé approximant overestimates the water vapor absorption at large absorber amounts compared with our line-by-line calculations. There are no comparisons made for the other intervals because of the different spectral regions.

The method first proposed by Rodgers and Walshaw (1966) is used to account for the temperature depen-

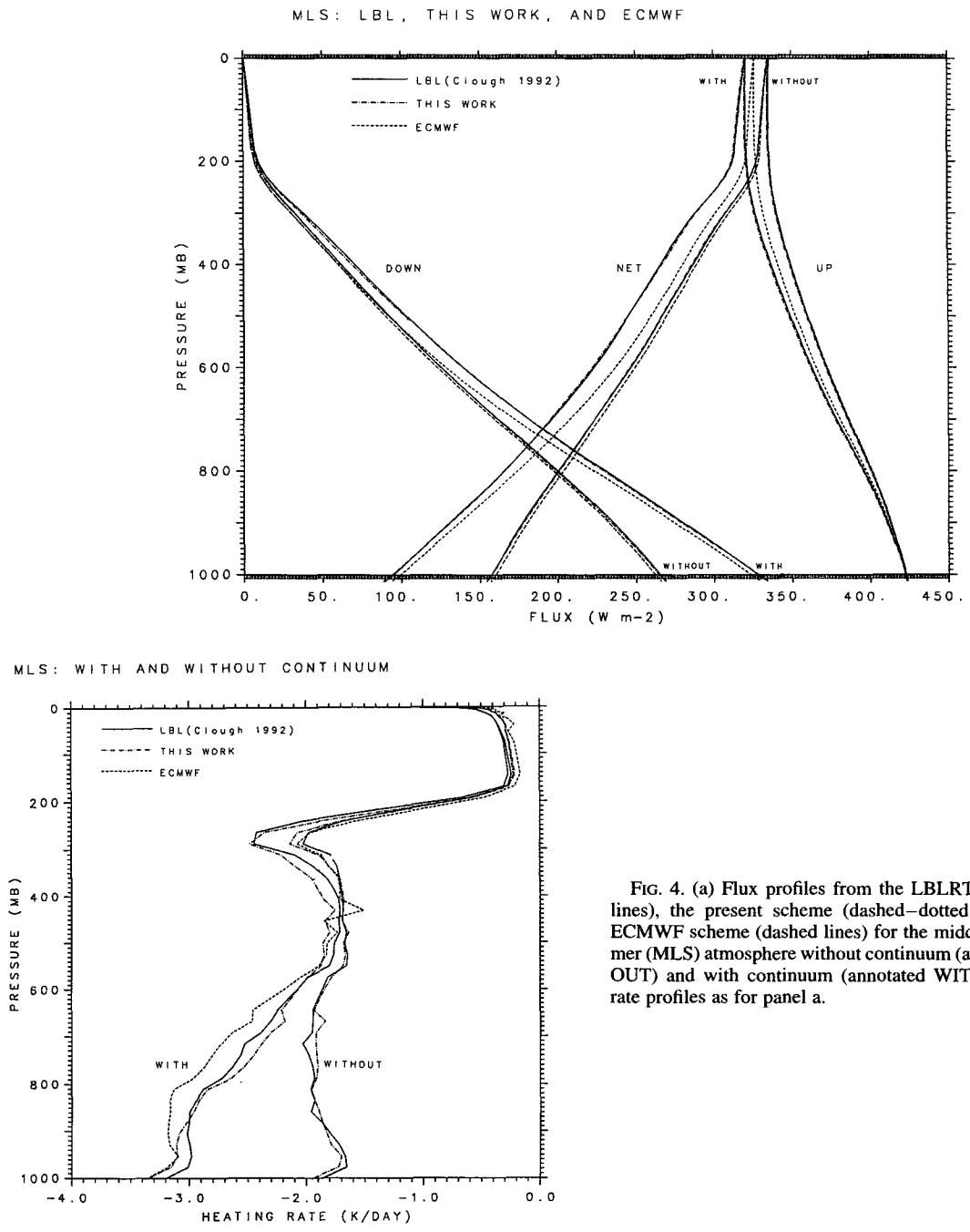

FIG. 4. (a) Flux profiles from the LBLRTM model (solid lines), the present scheme (dashed–dotted lines), and the ECMWF scheme (dashed lines) for the middle-latitude summer (MLS) atmosphere without continuum (annotated WITHOUT) and with continuum (annotated WITH). (b) Cooling rate profiles as for panel a.

dence with the adaptation of MSF, including a dependence on absorber amount

$$\Phi(T, up) = \exp[a(up)(T - 250) + b(up)(T - 250)^2], \quad (11)$$

where $a(up)$ and $b(up)$ are coefficients dependent on the absorber amount. Again, these parameters are found from the line-by-line calculations rather than NBM. The effective absorber amount, which is used to compute a transmissivity, is approximated by

$$(up)_e = \int_{p_1}^{p_2} \Phi(T, up) p du. \quad (12)$$

Ramanathan and Downey drew attention to the error incurred by use of an isothermal emissivity formulation and demonstrated an accuracy of a non-isothermal emissivity method to be within 3% in cooling rates and 1.5% in fluxes. In order to incorporate the temperature dependence due to Wien's displacement law (i.e., the dependence of t on T_p),

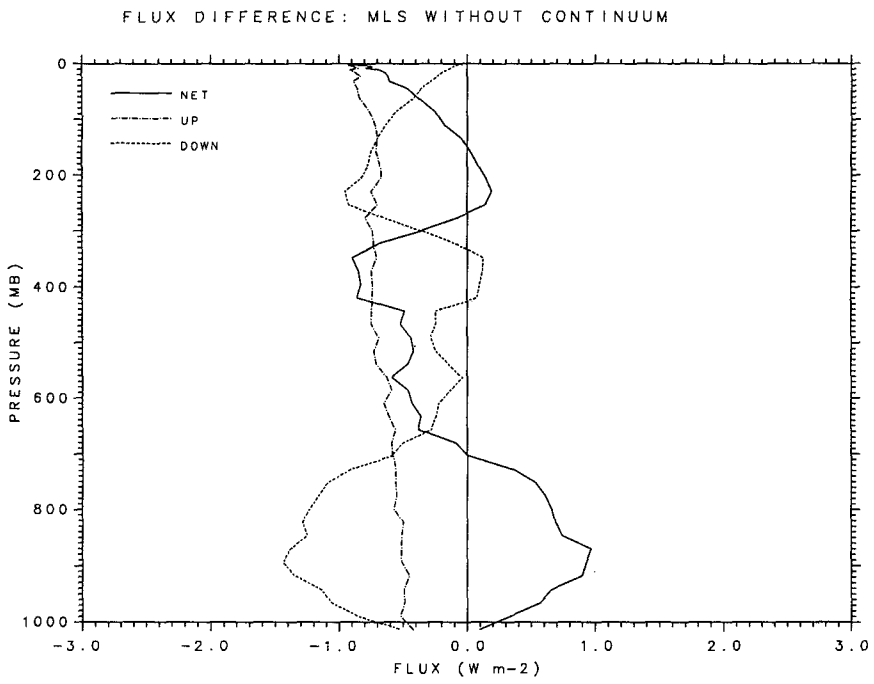

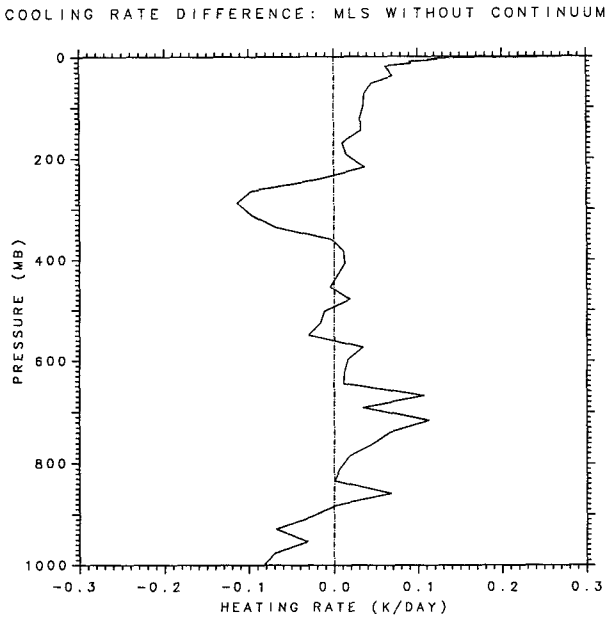

FIG. 5. (a) Flux difference profiles between the present scheme and LBLRTM model for the MLS atmosphere without continuum. The solid line is the net flux difference, the dashed–dotted line is the upward flux difference, and the dashed line is the downward flux difference. (b) Cooling rate difference profiles as for panel a.

we fit the coefficients in Eq. (8) for 11 temperatures between 187.5 and 312.5 K with a 12.5-K increment, and the transmissivities are computed using what is closest to the emitting level temperature T_p (i.e., no interpolation is required). Figure 2 shows the emissivities in interval 1880–3000 cm^{-1} for the 11 values of T_p. For eight intervals there are altogether 66 $\times$ 10 coefficients for Eq. (9) and 66 coefficients for calculating $a(up)$ and $b(up)$ in Eq. (11). Those who are interested in using the coefficients may obtain them from the authors.

5. Water vapor continuum

Radiative fluxes due to the water vapor continuum contribute significantly to tropospheric heating rates, especially in the Tropics and middle latitudes. Based on the Van Vleck and Huber (1977) formalism, Clough et al. (1980) proposed a formulation for the broadened line shape and a water vapor continuum model. More recently the water vapor continuum model was described by Clough et al. (1989) and has been used in their line-by-line program LBLRTM (Line-By-Line

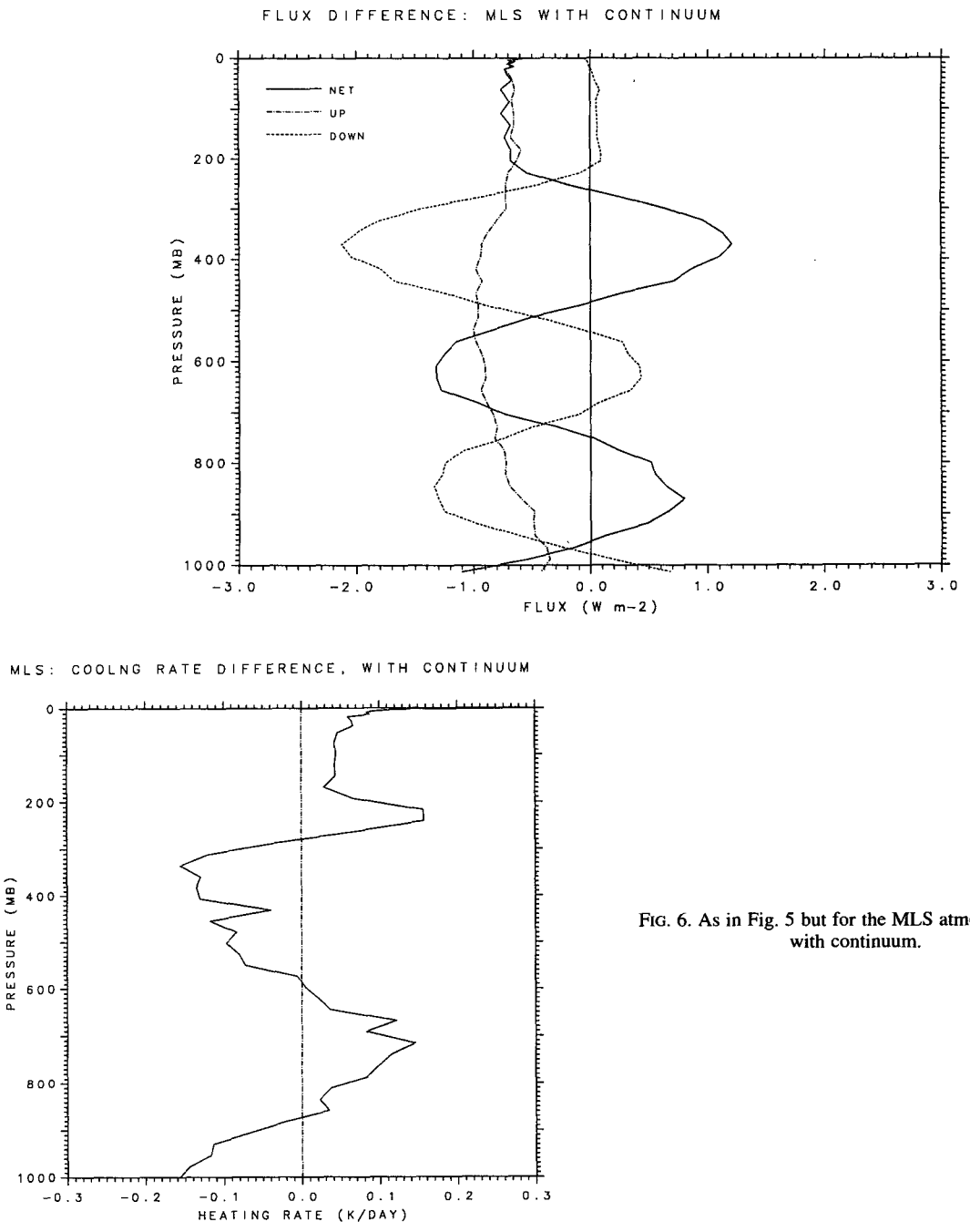

FIG. 6. As in Fig. 5 but for the MLS atmosphere case with continuum.

Radiative Transfer Model, previously referred to as FASCODE). Clough et al. have demonstrated that the continuum is important across the whole infrared spectrum, and that their line shape formulation and definition of associated continuum satisfy both e-type (self) and p-type (foreign) broadening at all frequencies. The self-broadened continuum at temperatures 260 and 296 K and the foreign-broadened continuum at 296 K have been precomputed using their semiempirical model. Recently, Ma and Tipping (1992) have developed a quasi-static model from first principles, which gives a temperature dependence in essential agreement with the CKD model.

Using line-by-line calculations Clough et al. (1992) found that the foreign-broadened continuum makes a significant contribution to water vapor absorption in the strong intervals 50–300 and 1400–1800 cm^{-1} and is more important in upper troposphere and colder polar regions, while the self-broadened continuum dominates in the atmospheric window region, 700–1300 cm^{-1},

and is more important in the lower troposphere. Because of a lack of sufficiently accurate measurements of the continuum in some spectral intervals and for some temperatures, the continuum values should be the subject of continuing refinement through spectral atmospheric measurements.

Most of the existing longwave radiation schemes used in climate models employ, for the water vapor continuum, the formulation of Roberts et al. (1976, hereafter RSB), mainly because of its simplicity. We are not aware of any parameterization that has employed the CKD water vapor continuum model in a radiation scheme suitable for implementation in climate models. In this paper, we use the CKD model to calculate the self-broadened (k^s) and foreign-broadened (k^f) absorption coefficients as a function of water vapor partial pressure (e) and total pressure (p):

$$k_\nu^s(e, T) = \nu \tanh\left(\frac{hc\nu}{2kT}\right)\left(\frac{296}{T}\right)eC_s(\nu, T), \quad (13)$$

$$k_\nu^f(p - e, T) = \nu \tanh\left(\frac{hc\nu}{2kT}\right)\left(\frac{296}{T}\right)(p - e)C_f(\nu, T), \quad (14)$$

where C_s and C_f are the self- and foreign-broadened continuum functions, respectively, which are dependent on wavenumber and temperature; C_s and C_f have been obtained by Clough et al. and stored in the line-by-line model at 10-cm^{-1} intervals. Because of the slow variation of the coefficients with wavelength, for the monochromatic values needed for the line-by-line method an interpolation is used.

The self- and foreign-broadened continua weighted by Planck's function and its derivative are calculated, according to Eqs. (13)–(16), using the GENLN2 line-by-line model for the eight spectral intervals at a temperature of 296 K:

$$ts_{B_i}^d(ue, T_p) = \frac{2\int_{\Delta\nu_i} B_\nu(T_p)\int_0^1 \exp[-k_\nu^s(e, 296)u/\mu]\mu d\mu d\nu}{\int_{\Delta\nu_i} B_\nu(T_p)d\nu}$$

$$ts_{dB_i}^d(ue, T_p) = \frac{2\int_{\Delta\nu_i} \frac{dB_\nu(T_p)}{dT}\int_0^1 \exp[-k_\nu^s(e, 296)u/\mu]\mu d\mu d\nu}{\int_{\Delta\nu_i} \frac{dB_\nu(T_p)}{dT} d\nu} \quad (15)$$

and

$$tf_{B_i}^d(u(p - e), T_p) = \frac{2\int_{\Delta\nu_i} B_\nu(T_p)\int_0^1 \exp[-k_\nu^f(p - e, 296)u/\mu]\mu d\mu d\nu}{\int_{\Delta\nu_i} B_\nu(T_p)d\nu}$$

$$tf_{dB_i}^d(u(p - e), T_p) = \frac{2\int_{\Delta\nu_i} \frac{dB_\nu(T_p)}{dT}\int_0^1 \exp[-k_\nu^f(p - e, 296)u/\mu]\mu d\mu d\nu}{\int_{\Delta\nu_i} \frac{dB_\nu(T_p)}{dT} d\nu}. \quad (16)$$

According to the CKD model the temperature dependence of the water vapor continuum is a function of frequency; we use an average wavenumber for each interval and the following expression for the self-broadened continuum:

$$f_i^s(T) = \bar{C}_s^i(T)/\bar{C}_s^i(296) = \exp\left[\Theta_i\left(1 - \frac{T}{296}\right)\right], \quad (17)$$

where

$$\Theta_i = \frac{296}{296 - 260}\ln\left[\frac{\bar{C}_s^i(260)}{\bar{C}_s^i(296)}\right], \quad (18)$$

where the sub/superscript i represents the ith interval. The ratios used for the intervals are listed in the Table 2. Our comparison shows that the CKD model has a similar temperature dependence to the RSB model for higher temperatures but a weaker dependence at lower temperatures. For the foreign-broadened continuum the

TABLE 3. Parameters of the water vapor self-broadened continuum.

Interval (cm^{-1})	$a_s(T_p)$ (g^{-1} cm^2) 187.5 K	200.0 K	212.5 K	225.0 K	237.5 K	250.0 K	262.5 K	275.0 K	287.5 K	300.0 K	312.5 K	b_s (g^{-1} cm^2)	c_s (g^{-1} cm^2)
0–350 + 1450–1880 ϵ_1	1178.11	1108.77	1044.99	987.37	935.91	890.38	850.38	815.50	785.25	759.14	736.69	150.0	5.0
0–350 + 1450–1880 ϵ_2	996.24	924.99	864.44	813.88	772.35	738.66	711.54	689.77	672.23	658.02	646.40		
350–500 ϵ_1	285.28	284.92	284.60	284.32	284.08	283.87	283.69	283.52	283.37	283.23	283.09	42.0	15.5
350–500 ϵ_2	283.63	283.32	283.03	282.76	282.52	282.33	282.15	282.00	281.87	281.75	281.64		
500–650 ϵ_1	98.88	98.58	98.32	98.09	97.90	97.72	97.57	97.43	97.30	97.19	97.09	17.5	7.0
500–650 ϵ_2	97.84	97.56	97.33	97.13	96.95	96.80	96.67	96.55	96.44	96.35	96.27		
650–800 ϵ_1	39.02	38.85	38.71	38.59	38.48	38.38	38.30	38.22	38.15	38.09	38.03	9.5	4.2
650–800 ϵ_2	38.56	38.40	38.27	38.15	38.05	37.96	37.89	37.82	37.75	37.70	37.65		
800–970 ϵ_1	16.53	16.45	16.38	16.31	16.26	16.21	16.16	16.12	16.09	16.05	16.02	7.1	3.8
800–970 ϵ_2	16.34	16.26	16.19	16.13	16.07	16.03	15.98	15.95	15.91	15.88	15.85		
970–1110 ϵ_1	7.04	7.03	7.02	7.02	7.01	7.01	6.99	6.99	6.99	6.98	6.98	0.0	0.0
970–1110 ϵ_2	7.02	7.01	7.00	6.99	6.99	6.98	6.97	6.97	6.96	6.96	6.95		
1110–1250 ϵ_1	6.46	6.47	6.48	6.49	6.49	6.50	6.50	6.51	6.51	6.52	6.52	0.0	0.0
1110–1250 ϵ_2	6.48	6.49	6.50	6.50	6.51	6.52	6.53	6.53	6.53	6.54	6.54		
1250–1350 ϵ_1	16.75	16.81	16.86	16.91	16.95	16.99	17.03	17.06	17.09	17.12	17.14	7.45	3.45
1250–1350 ϵ_2	16.84	16.91	16.96	17.01	17.05	17.09	17.13	17.16	17.19	17.22	17.24		
1350–1450 ϵ_1	68.47	68.66	68.84	68.99	69.13	69.26	69.38	69.48	69.58	69.67	69.75	16.1	5.2
1350–1450 ϵ_2	68.76	68.96	69.14	69.29	69.44	69.57	69.68	69.78	69.89	69.98	70.06		
1880–3000 ϵ_{11}	12.92	12.19	11.52	10.92	10.37	9.87	9.42	9.00	8.62	8.27	7.94	9.0	1.0
1880–3000 ϵ_2	12.20	11.45	10.77	10.16	9.61	9.10	8.65	8.23	7.85	7.50	7.19		

TABLE 4. Parameters of the water vapor foreign-broadened continuum.

Interval (cm^{-1})	$a_f(T_p)$ (g^{-1} cm^2) 187.5 K	200.0 K	212.5 K	225.0 K	237.5 K	250.0 K	262.5 K	275.0 K	287.5 K	300.0 K	312.5 K	b_f (g^{-1} cm^2)	c_f (g^{-1} cm^2)
0–350 + 1450–1880 ϵ_1	76.577	73.332	70.449	67.895	65.641	63.661	61.930	60.424	59.119	57.994	57.025	9.0	0.3
0–350 + 1450–1880 ϵ_2	68.422	65.313	62.687	60.501	58.705	57.245	56.066	55.114	54.342	53.713	53.194		
350–500 ϵ_1	6.982	6.955	6.933	6.913	6.896	6.881	6.868	6.856	6.845	6.836	6.827	2.0	0.34
350–500 ϵ_2	6.864	6.842	6.823	6.807	6.793	6.781	6.771	6.762	6.754	6.747	6.741		
500–650 ϵ_1	0.586	0.580	0.575	0.571	0.567	0.563	0.560	0.558	0.555	0.553	0.551	0.27	0.066
500–650 ϵ_2	0.565	0.560	0.555	0.552	0.548	0.545	0.543	0.540	0.538	0.537	0.535		
650–800 ϵ_1	0.052	0.052	0.051	0.051	0.050	0.050	0.050	0.050	0.049	0.049	0.049	0.095	0.057
650–800 ϵ_2	0.051	0.050	0.050	0.049	0.049	0.049	0.049	0.048	0.049	0.048	0.048		
800–970 ϵ_1	0.017	0.017	0.017	0.017	0.017	0.017	0.017	0.017	0.017	0.017	0.017	0.0	0.0
800–970 ϵ_2	0.017	0.017	0.017	0.017	0.017	0.017	0.017	0.017	0.017	0.017	0.017		
970–1110 ϵ_1	0.017	0.017	0.017	0.017	0.017	0.017	0.017	0.017	0.017	0.017	0.017	0.0	0.0
970–1110 ϵ_2	0.017	0.017	0.017	0.017	0.017	0.017	0.017	0.017	0.017	0.017	0.017		
1110–1250 ϵ_1	0.038	0.039	0.039	0.039	0.040	0.040	0.040	0.040	0.040	0.041	0.041	0.0	0.0
1110–1250 ϵ_2	0.039	0.039	0.040	0.040	0.040	0.041	0.041	0.041	0.041	0.041	0.042		
1250–1350 ϵ_1	0.740	0.746	0.750	0.755	0.759	0.762	0.765	0.768	0.771	0.774	0.776	0.44	0.086
1250–1350 ϵ_2	0.749	0.754	0.759	0.764	0.768	0.771	0.775	0.778	0.780	0.783	0.785		
1350–1450 ϵ_1	6.721	6.733	6.744	6.754	6.763	6.771	6.778	6.785	6.791	6.796	6.802	1.29	0.31
1350–1450 ϵ_2	6.739	6.752	6.763	6.773	6.782	6.790	6.797	6.804	6.810	6.816	6.821		
1880–3000 ϵ_1	0.852	0.800	0.753	0.711	0.674	0.641	0.611	0.584	0.559	0.537	0.516	0.71	0.035
1880–3000 ϵ_2	0.800	0.748	0.701	0.660	0.623	0.590	0.561	0.534	0.510	0.488	0.468		

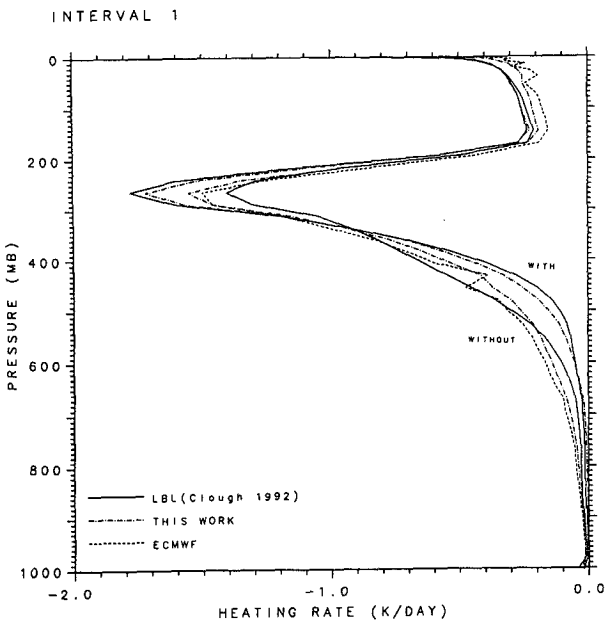

FIG. 7. Cooling rate profiles from the LBLRTM model (solid lines), the present scheme (dashed–dotted lines), and the ECMWF scheme (dashed lines) for the interval 0–350 + 1450–1880 cm^{-1} without continuum and with continuum.

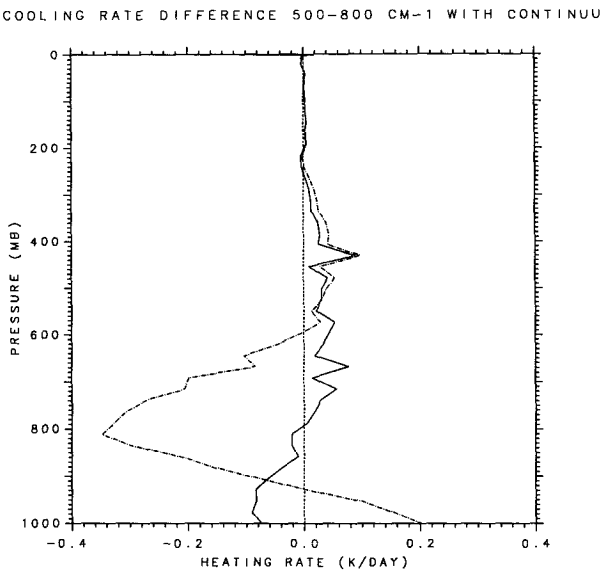

FIG. 8. Cooling rate difference between the present scheme and the LBLRTM model from one band (dashed–dotted line) and two bands (solid line) overlapping in the interval 500–800 cm^{-1}.

temperature dependence is almost independent of frequency, and we have used a simple inverse-temperature relationship in the parameterization.

To parameterize the calculated water vapor continuum the following expressions are used:

$$tc_i = \exp[-\overline{k_{s_i}}(T_p)\overline{ue} - \overline{k_{f_i}}(T_p)\overline{u(p-e)}], \quad (19)$$

where

$$\overline{ue} = \int_{u(p_1)}^{u(p_2)} e(p) f_i^s(T)\, du(p) \quad (20)$$

$$\overline{u(p-e)} = \int_{u(p_1)}^{u(p_2)} (p - e(p)) f_i^f(T)\, du(p), \quad (21)$$

and

$$\overline{k_{s_i}}(T_p) = a_{s_i}(T_p)\frac{1 + c_{s_i}\overline{ue}}{1 + b_{s_i}\overline{ue}} \quad (i = 1, 2, 3, 4, 7, 8)$$

$$\overline{k_{s_i}}(T_p) = a_{s_i}(T_p) \quad (i = 5, 6). \quad (22)$$

For the foreign-broadened continuum the following formulas can be used:

$$\overline{k_{f_i}}(T_p) = \begin{cases} a_{f_i}(T_p)\dfrac{1 + c_{f_i}\overline{u(p-e)}}{1 + b_{f_i}\overline{u(p-e)}}, & i = 1, 2, 3, 7, 8 \\ a_{f_i}(T_p), & i = 4, 5, 6, \end{cases} \quad (23)$$

where the coefficients b_{s_i}, c_{s_i}, b_{f_i}, and c_{f_i} are constants, and $a_{s_i}(T_p)$ and $a_{f_i}(T_p)$ are obtained by a least squares method (see Tables 3 and 4). Figure 3 shows the optical depth as a function of pressure-weighted absorber amount for the self- and foreign-broadened continuum, respectively, and the LSF for each interval. For the interval 500–800 cm^{-1} it is found necessary to divide into subintervals 500–650 and 650–800 cm^{-1} to accurately incorporate the overlap between continuum and absorption lines considering the large variation of the continuum absorption coefficient. Because in the 500–800 cm^{-1} interval line absorption has been included, the total transmissivity is calculated by the following equation, which is similar to the approach used by RD:

$$t = 0.5[t_{l_1} tc_1 + (2t_l - t_{l_1})tc_2], \quad (24)$$

where t_l and t_{l_1} represent the transmissivities due to lines in the intervals 500–800 and 500–650 cm^{-1} respectively, while tc_1 and tc_2 represent the transmissiv-

TABLE 5. Maximum errors in downward flux and cooling rate from the band-by-band comparison with Clough et al.'s MLS with continuum line-by-line calculation.

Interval	Max$\Delta F\downarrow$ (W m^{-2})	Level of max$\Delta F\downarrow$	MaxΔQ (K/d)	Level of maxΔQ
0–350 + 1450–1880	−0.6	250 mb	0.08	300 mb
500–800	1.5	800 mb	−0.09	700 mb
800–970	−0.72	800 mb	−0.065	surface
1110–1250	−0.35	surface	−0.02	surface
970–1110	0.7	900 mb	0.015	800 mb
350–500	−1.4	650 mb	−0.12	450 mb
1250–1450	−0.3	700 mb	0.02	840 mb
1880–2820	0.47	surface	−0.02	surface

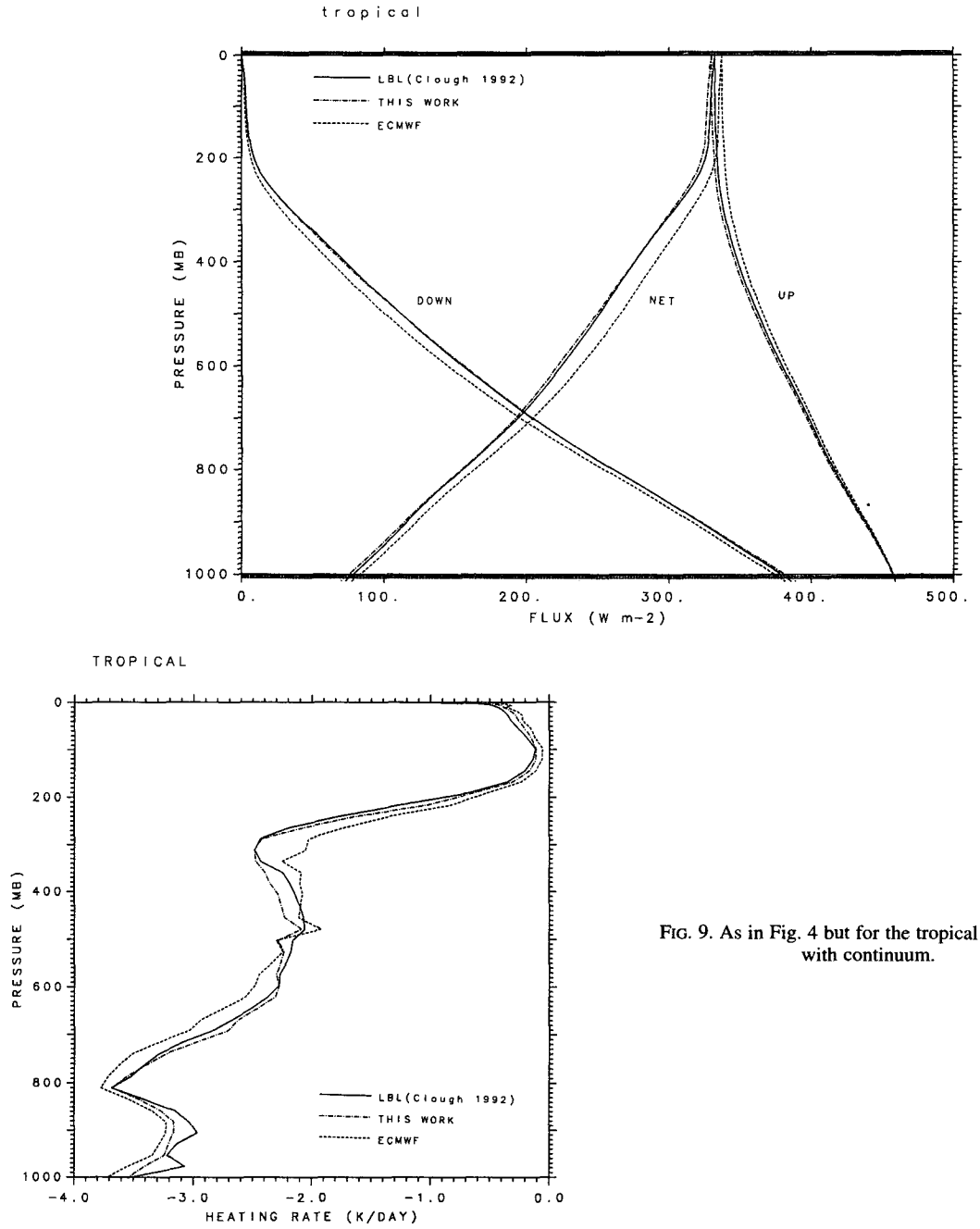

FIG. 9. As in Fig. 4 but for the tropical atmosphere with continuum.

ities due to continuum absorption in the intervals 500–650 and 650–800 cm^{-1}, respectively. We also found that it is necessary to split the interval 1250–1450 cm^{-1} for the same reason.

We have fitted the continuum for 11 emitting temperatures of T_p for the eight intervals, but for weaker and narrower intervals, 970–1110 and 1110–1250 cm^{-1} (self- and foreign-broadened) and 800–970 cm^{-1} (foreign-broadened), only one T_p (262.5 K) is used in the scheme to reduce computational demands.

6. Results and comparison of longwave fluxes and cooling rates

The Clough et al. (1992) line-by-line calculations of atmospheric fluxes and cooling rates for water vapor are used as a benchmark against which to compare our emissivity scheme results. Sixty layers, the same as described by Clough et al., are used for the vertical integration. Figure 4a shows a comparison of fluxes integrated across the entire spectrum for the ICRCCM

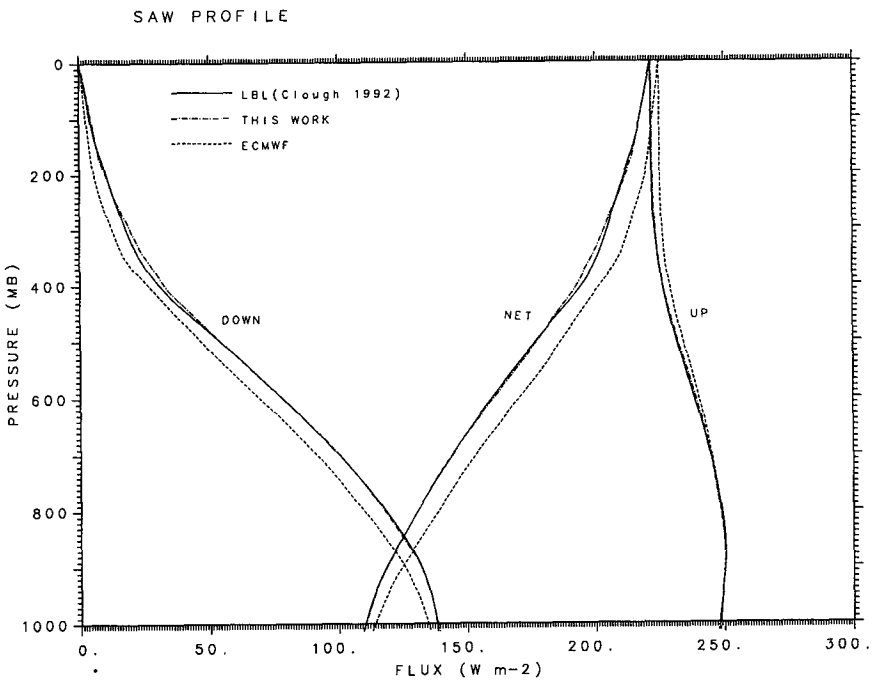

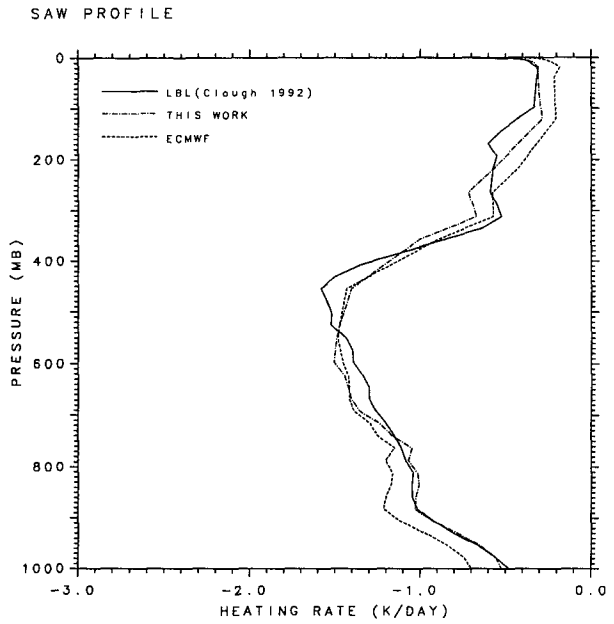

FIG. 10. As in Fig. 4 but for the subarctic winter atmosphere with continuum.

(Ellingson et al. 1991) middle-latitude summer temperature and water vapor profiles (without and with continuum). The Clough et al. line-by-line calculations are the solid line, our results are the dash–dotted line, and the dashed line shows ECMWF results; Fig. 4b shows the equivalent heating rates. It can be seen that our scheme has improved the fluxes (without continuum) by 1 to 2 W m^{-2} over the ECMWF results. In Fig. 5 are shown the differences between the results of our scheme and the Clough et al. calculations; the solid curve in Fig. 5a represents the net flux difference, the dash–dotted curve the upward flux difference, and the dotted curve the downward flux difference. It can be seen that the maximum error in downward flux for middle-latitude summer profile without continuum case in our scheme is less than 1 W m^{-2} and less than 1.5 W m^{-2} in net flux, which represents a relative error of better than 1%. The maximum error in our scheme in the cooling rate for water vapor lines only is 0.11 K/d, which appears in the upper troposphere and near 700 mb; the general error is within 0.1 K/d or 5%. When the continuum is included the maximum error is less

TABLE 6. Comparison of fluxes (in W/m^{-2}) from the present work, the Clough et al. line-by-line model, and the ECMWF scheme.

	Line-by-line		This work		ECMWF	
Top	up		up		up	
Midlatitude summer (without)	335.7		335.3		335.0	
Midlatitude summer (with)	321.0		320.3		326.4	
Tropical (with)	332.6		330.2		337.4	
Subarctic winter (with)	221.5		221.7		224.5	
Tropopause	up	down	up	down	up	down
Midlatitude summer (without)	335.8	7.0	335.7	6.2	335.5	5.4
Midlatitude summer (with)	321.2	7.4	320.6	7.5	326.9	5.4
Tropical (with)	332.5	3.4	330.2	3.2	337.2	2.4
Subarctic winter (with)	222.4	16.2	222.5	13.0	225.2	10.8
Surface	up	down	up	down	up	down
Midlatitude summer (without)	423.3	269.0	422.9	268.9	423.0	265.9
Midlatitude summer (with)	423.5	333.9	423.1	334.6	423.2	329.4
Tropical (with)	458.9	385.9	458.8	389.1	458.9	381.5
Subarctic winter (with)	247.6	138.2	247.7	138.5	247.7	135.3

than 1.4 W m^{-2} in downward flux and less than 2.1 W m^{-2} in net flux; the maximum error in cooling rate is 0.16 K day^{-1} (see Fig. 6).

A band-by-band comparison has also been conducted for the middle-latitude summer atmosphere. In general, the agreement between our emissivity calculation and the line-by-line results is very good. Figures 7 and 8 show two examples of the comparison of fluxes and cooling rates between the Clough et al. line-by-line calculations and the present work for two of our eight intervals. The solid line in Fig. 7 is the Clough et al. cooling rate for the strong band of 10–350 + 1450–1880 cm^{-1} with and without continuum, and the dash-dotted line is the present parameterization result for the band. The maximum error of our model in cooling rate never exceeds 0.08 K/d, and that in fluxes within 0.6 W m^{-2}. The contribution of continuum to cooling rate reaches 0.3 K/d between 250 and 300 mb mainly due to the foreign-broadened continuum, which also causes less cooling in the lower troposphere. The dashed curve in Fig. 7 shows the ECMWF cooling rate.

In the interval 500–800 cm^{-1} (Fig. 8) the maximum error in cooling rate is less than 0.09 K/d and the error in flux within 1.5 W m^{-2}, using the two subintervals to deal with the overlap of the continuum with the absorption lines. Without the subintervals the maximum errors caused by the overlap in the 300 cm^{-1} wideband approach about 0.35 K/d in cooling rate and 7.5 W m^{-2} in flux. Table 5 gives the maximum errors in downward fluxes and for all intervals and the pressure levels at which these occur.

Figures 9 and 10 show a comparison between the present parameterization and the line-by-line calculation of fluxes and cooling rates for standard tropical and subarctic winter atmospheres (as used by Clough et al. 1992). The ECMWF fluxes and cooling rates are also shown. In general the agreement between our calculations and the line-by-line results are very good; the difference is generally within 2 W m^{-2} in flux and within 0.2 K/d in cooling rate. The difference in fluxes between ECMWF and the line-by-line results is larger than 10 W m^{-2} in most of the troposphere because the RSB continuum model is employed in the former. Even in the SAW case, where the water vapor densities are very low, the flux difference remains quite large; this indicates that the foreign-broadened continuum plays an important part in the colder atmosphere. As in the MLS case the RSB continuum model causes about 0.2 K/d more cooling in the lower troposphere and around 0.3 K/d less cooling in the upper troposphere compared with the Clough et al. line-by-line results. Figure 10a shows the significant improvement in fluxes produced by our new scheme but some slight difference in slope results in the little improvement in cooling rate in the middle and upper troposphere (Fig. 10b). Errors here are due to the treatment of the temperature dependence of the spectral lines (not the continuum) in the interval 1 (0–350 + 1450–1880 cm^{-1}) exacerbated by the discontinuities in the temperature lapse rate present in the SAW profile. Changing the resolution of the vertical integration appears to ameliorate this problem, and we are investigating it further.

Table 6 gives a comparison of fluxes at the surface, the tropopause, and the top of the atmosphere. It can be seen that there are improvements in downward flux in both the lines only (without continuum) and in the total.

7. Summary and conclusions

We have presented a new approach to the emissivity method based on line-by-line model calculations. The approach does not use narrowband models and the strong line approximation as intermediate tools. Nonisothermal diffuse transmissivities weighted by the Planck function and its derivative are developed from the GENLN2 line-by-line model for a variety of homogeneous atmospheric paths. A simple Padé-like formula is directly fitted to the line-by-line reference calculations for wide spectral intervals by a least squares method while the correct pressure and temperature dependence of the transmissivities is maintained. A comparison of the results of this new parameterization with the LBLRTM line-by-line computed fluxes and heating rates for the MLS atmosphere without including continuum absorption shows that the agreement is within 1% in fluxes and within 5% in cooling rates. The water vapor continuum transmissivities have been computed using the Clough et al. (1989) model, and parameterizations of the self-broadened and foreign-broadened

continua have been included over the entire infrared spectrum. Comparison of the new parameterization with LBLRTM fluxes and cooling rates including the continuum absorption for different atmospheric profiles shows that the agreement in fluxes is within 2–3 W m^{-2} and within 10% in cooling rates.

The increase of CPU time from the ECMWF six-interval water vapor scheme to our eight-interval water vapor scheme would be about 33%, considering only the number of intervals. Taking into account the CPU time used for carbon dioxide and ozone and other common calculations, however, the increase of computational costs is less than 20%. The CPU usage of the ECMWF six-interval scheme for a gridpoint calculation with the 19-level model on a supercomputer is documented by Morcrette (1991).

We have also replaced the Padé approximant of carbon dioxide 15 μm and the band model of ozone 9.6 μm in the ECMWF longwave radiation scheme by transmission tables calculated using the line-by-line model. Other trace gases such as CH_4, N_2O, and CFCs can easily be incorporated into the scheme. The scheme is suitable for use in GCMs or chemical climate models. For reasons of space constraints and because detailed line-by-line heating rate calculations are not available for comparison, we have not included examples of these calculations here, but we intend to carry out such a comparison and to investigate the impact of the whole new scheme in a suite of GCMs as part of the U.K. Universities Global Atmospheric Modeling Program (UGAMP). We also intend to make further comparisons between our theoretical results and in situ and remote measurements of radiative fluxes.

Note added in proof. Since the writing of this paper, Clough and Coworkers (1994, personal communication) have refined the parameters in the CKD model. This has no effect on the theoretical aspects of our paper but may result in slightly different values than those appearing in Tables 3 and 4 and Fig. 3 (mainly in the window region). These are presently being reworked.

Acknowledgments. The authors would like to thank the Department of Atmospheric, Oceanic and Planetary Physics, Oxford University, and David Edwards (NCAR) for permission to use the GENLN2 line-by-line program. We are grateful to Jean-Jacques Morcrette for providing the ECMWF radiation scheme and to Shepard Clough and Michael Iacono for access to results from the LBLRTM model. Thanks also go to Ken Bignell for helpful discussions. This work was supported by the U.K. Department of the Environment and by the Natural Environment Research Council's UGAMP project.

REFERENCES

Chou, M.-D., and A. Arking, 1980: Computation of infrared cooling rates in the water vapor bands. *J. Atmos. Sci.*, **37,** 855–867.

Clough, S. A., F. X. Kneizys, R. W. Davies, R. Gamache, and R. H. Tipping, 1980: Theoretical line shape for H_2O vapor: Application to the continuum. *Atmospheric Water Vapor,* A. Deepak, T. D. Wilkerson, and L. H. Rhimke, Eds., Academic Press, 25–46.

——, ——, and ——, 1989: Line shape and the water vapor continuum. *Atmos. Res.*, **23,** 229–241.

——, M. J. Iacono, and J.-L. Moncet, 1992: Line-by-line calculations of atmospheric fluxes and cooling rates: Application to water vapor. *J. Geophys. Res.*, **97,** 15 761–15 785.

Edwards, D. P., 1987: GENLN2: The new Oxford line-by-line atmospheric transmission/radiance model. Memo. 87.2. Dept. of Atmospheric, Oceanic and Planetary Physics, University of Oxford, 87.2.

——, 1988: Atmospheric transmittance and radiance calculation using line-by-line computer models. *SPIE 928, Modeling of the Atmosphere,* 94–116.

Ellingson, R. G., J. Ellis, and S. Fels, 1991: The intercomparison of radiation codes used in climate models: Longwave results. *J. Geophys. Res.*, **96,** 8929–8953.

Fouquart, Y., and B. Bonnel, 1980: Computations of solar heating of the Earth's atmosphere: A new parameterization. *Beitr. Phys. Atmos.*, **53,** 35–62.

Garand, L., 1983: Some improvements and complements to the infrared emissivity algorithm including a parameterization of the absorption in the continuum region. *J. Atmos. Sci.*, **40,** 230–244.

Goody, R. M., and Y. L. Yung, 1989: *Atmospheric Radiation.* Oxford University Press, 519 pp.

Ma, Q., and R. H. Tipping, 1992: A far wing line shape theory and its application to the water continuum absorption in the infrared region (II). *J. Chem. Phys.*, **96,** 8655–8663.

Malkmus, W., 1967: Random Lorentz band model with exponential-tailed s^{-1} line intensity distribution function. *J. Opt. Soc. Amer.*, **57,** 323–329.

Morcrette, J.-J., 1989: Description of the radiation scheme in the ECMWF model. ECMWF Research Dept. Tech. Memo. 165, 26 pp.

——, 1991: Radiation and cloud radiative properties in the European Centre for Medium-Range Weather Forecasts forecasting system. *J. Geophys. Res.*, **96,** 9121–9132.

——, L. Smith, and Y. Fouquart, 1986: Pressure and temperature dependence of the absorption in longwave radiation parameterization. *Beitr. Phys. Atmos.*, **59,** 455–469.

Ramanathan, V., and Downey, 1986: A non-isothermal emissivity and absorptivity formulation. *J. Geophys. Res.*, **91,** 8649–8666.

Roberts, R. E., J. E. A. Selby, and L. M. Biberman, 1976: Infrared continuum absorption by atmospheric water vapor in the 8–12 μm window. *Appl. Opt.*, **15,** 2085–2090.

Rodgers, C. D., 1967: The use of emissivity in atmospheric radiation calculations. *Quart. J. Roy. Meteor. Soc.*, **93,** 43–54.

——, and C. D. Walshaw, 1966: The computation of infrared cooling rate in planetary atmosphere. *Quart. J. Roy. Meteor. Soc.*, **92,** 67–92.

Rothman, L. S., R. R. Gamache, A. Goldman, L. R. Brrow, R. A. Toth, H. M. Pickett, R. L. Poynter, J.-M. Flaud, C. Camy-Peyret, A. Barbe, N. Husson, C. P. Rinsland, and M. A. H. Smith, 1987: The HITRAN database: 1986 edition. *Appl. Opt.*, **26**(19), 4058–4097.

Van Vleck, J. H., and D. L. Huber, 1977: Absorption, emission and linebreadths: A semihistorical perspective. *Rev. Mod. Phys.*, **49,** p. 939.